Journal of Ceramic Processing Research. Vol. 26, No. 4, pp. 628~634 (2025)
(Received 26 March 2025, Received in revised form 27 May 2025, Accepted 2 June 2025)
https://doi.org/10.36410/jcpr.2025.26.4.628

J O U R N A L O F
Ceramic Processing Research

Systematic optimization of sol-gel synthesis parameters for SiO_2 nanoparticles derived from immature rice ash and sugarcane bagasse ash

M. Selva Prathipa[a,*] and Dr. A. Arivumangai[b]
[a]*Research Scholar, Civil Engineering Dept., Dr. MGR Education and Research Institute, Chennai-95*
[b]*Professor, Civil Engineering Dept., Dr. MGR Education and Research Institute, Chennai-95*

In this study, SiO_2 was extracted from immature rice ash (IRA) and Sugarcane bagasse ash (SBA) under various experimental circumstances, varying temperatures, amounts of NaOH, and dissolved time. Then, SiO_2 nanoparticles were created using the sol-gel method. By increasing the amount of time, the effects of the experimental circumstances are investigated. IRA and SBA were subjected to NaOH dissolution for 60, 90, 120, 150, and 180 minutes. A range of NaOH volumes 100 to 400 ml and temperatures (50 °C to 100 °C in 10 °C increments) were tested, keeping the biomass quantity constant at 10 g. Different experimental settings were used to calculate the amount of SiO_2 extracted, and optimum experimental conditions were used to perform the extraction process. The FTIR, SEM, and XRD are used to characterize the extracted SiO_2 nanoparticles. Results confirm the successful formation of high-purity SiO_2 nanoparticles, with IRA demonstrating a novel precursor source and process conditions tailored for both IRA and SBA. This work contributes to sustainable nanomaterial production by valorising underutilized agricultural waste.

Keywords: Immature rice ash, Sugarcane bagasse ash, Sol-gel method.

Introduction

A significant volume of solid agricultural waste, such as sugarcane bagasse and immature rice, can cause an accumulation of rubbish, which can harm the environment and cause health issues for people [1]. One of India's main agricultural products is sugarcane. Only animal feed, fertiliser, or repurposed fuel in sugar plants have been made from sugarcane bagasse, with the ashes being discarded [2]. In many rice-producing nations, one of the most frequently available agricultural wastes is immature rice, a result of the milling process. About 93.20% of silica in immature rice and 96.93% of the silica in sugarcane bagasse [3] Similar to other ligno cellulosic biomass feed stocks; it is composed of cellulose, hemicelluloses, and lignin, giving it a range of characteristics that make it suitable for use as a feedstock in the production of bioethanol [4]. Since immature rice is a waste product from the forestry and agriculture industries, it is practically free. Its use can help with waste treatment costs by lowering the need for waste disposal [5]. IRA is created when immature rice is burned. The primary agricultural waste products generated during the cultivation of rice are husk, flour, and straw. Straw is commonly burned in fields despite being more expensive to gather than rice and potentially harmful to the soil's fertile layer as well as the atmosphere [6]. Roughly 20 percent of the 600 million tonnes of rice produced annually are immature rice (RH), which has high silica content and cannot be used as animal feed since it does not burn or fully degrade [7]. The majority of the ash is made up of 87–97% silica, which is useful for industrial application due to its large exterior surface area, lightweight nature, and high porosity [8]. RHA contains trace amounts of K_2O, Al_2O_3, CaO, MgO, Na_2O, and Fe_2O_3, usually less than 1% [9]. Immature rice ranges in bulk density from 96 to 160 kg/m^3, and its levels of sulphur, nitrogen, and oxygen are, respectively, 31 to 37%, 0.23–0.32%, and 0.04–0.08% [10]. Because sugarcane roots are crucial in drawing silica from the soil and transferring it to shoots, SBA has a high concentration of silica and can be utilised as a source of silica nanoparticles [2]. A variety of agricultural wastes, including immature rice, wheat husk, maize cob, nut grass, sugarcane leaves and bagasse, are sources of silica [11]. As seen in Fig. 1, silica, also known as silicon dioxide, is a common oxide compound composed of linked silicon and oxygen atoms. A central region of its structure is made up of four oxygen atoms joined at a tetrahedral angle to silicon atoms. These tetrahedral structures combine to create a silica matrix that is quite big [12]. Pore sizes in silica can range from 5 to 3000 Å, and they can be amorphous or take the shape of more stable quartz. The silicon and oxygen atoms have a bond angle of 109.5 degrees and a length that fluctuates between 1.54 and 1.69 Å [13]. Amorphous or irregular

*Corresponding author:
Tel : 9176432834
E-mail: prathipa@apec.edu.in

structures can be created by varying the angle between silicon-oxygen-silicon bonds, or siloxane bonds, which can range from 120 to 180 deg. This angle can be changed by variations in bond energy. The distinctive features of silica are attributed to the diverse shapes and compositions that these oxygen bridges can adopt [14]. Nowadays, nanotechnology is extensively employed in many significant scientific and technological domains, including electronics, medicine, industry, etc. Synthesis and surface science have explored the development of ceramic nanoparticles with better qualities with great success, including silica, alumina, titania, zirconia, silicon nitride, silicon carbide, etc [15]. Although various agricultural residues such as rice husk, wheat straw, and sugarcane bagasse have been studied for silica extraction, this study uniquely focuses on IRA an underutilized biomass waste with high silica content. Unlike mature rice husk ash, the immature variant remains largely unexplored for nanoparticle synthesis. Furthermore, the present research offers a systematic optimization of key synthesis parameters, including dissolution time, NaOH volume, and temperature, tailored separately for IRA and SBA. This approach not only ensures higher yield and purity but also enhances the reproducibility and scalability of the synthesis method. While the synthesis pathway is based on known sol-gel techniques, this work distinguishes itself by integrating IRA as a precursor and establishing optimum process conditions for both IRA and SBA, thereby contributing novel insights into sustainable silica nanoparticle production. This study addresses that gap by utilizing IRA for silica nanoparticle synthesis and systematically optimizing process parameters for both IRA and SBA. The optimized conditions ensure higher yield and better material quality. Thus, while the extraction method aligns with previously reported techniques, the use of IRA and the tailored experimental design offer novelty and practical value.

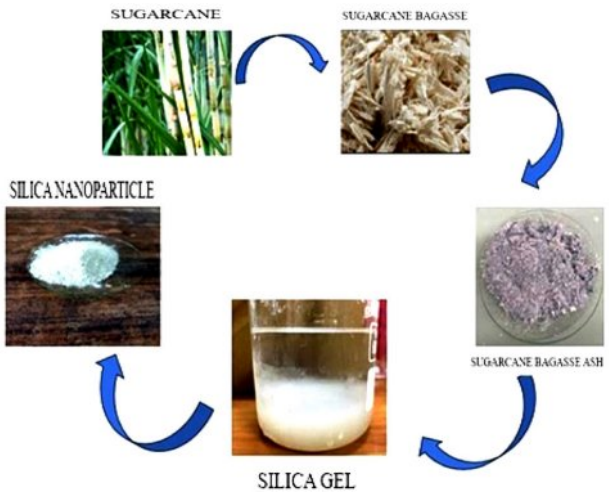

Fig. 1. Process of extraction of silica nanoparticles from sugarcane bagasse ash.

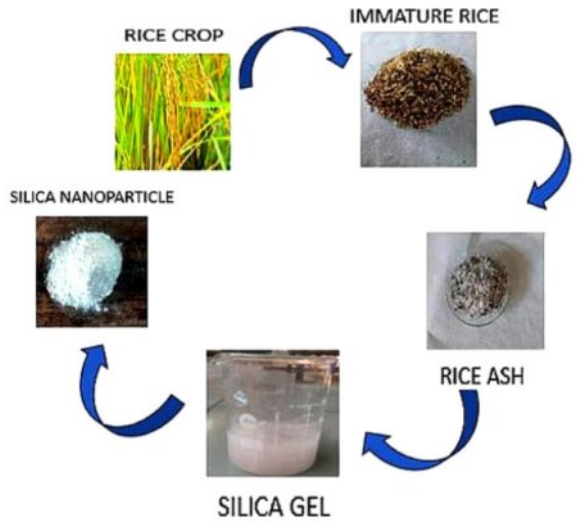

Fig. 2. Process of extraction of Silica nanoparticles from Immature Rice ash.

Materials and Methods

After being cleaned and dried, the IRA and sugarcane bagasse were chopped into smaller pieces. Both IRA and SBA were cleaned, dried, and calcined at 650 °C for 3 hours in a muffle furnace. For dissolution experiments, 10 g of ash was treated with 100 to 400 ml of NaOH and stirred for 1 hour. Experiments were conducted at temperatures ranging from 50 °C to 100 °C (10 °C intervals) to evaluate temperature effects. Samples were filtered, neutralized to pH 7 with HCl, and aged to form aqua gel, then washed, dried, and ground to obtain silica nanoparticles [16]. This study uniquely focuses on optimizing these parameters for both IRA and SBA, ensuring the most efficient recovery of high-purity silica nanoparticles.

Result and Discussions

Effect of Time

Figure 3 shows that the silica nanoparticle yield for immature rice peaks at around 60 minutes, followed by only a slight increase over time. This suggests that most of the extractable material is broken down early in the process, with minimal improvements afterward. While longer extraction times generally enhance yield, excessively long durations can lead to material degradation or saturation, ultimately reducing efficiency and stabilizing the yield [17]. In contrast, the highest yield of silica nanoparticles from sugarcane bagasse is achieved after 90 minutes, followed by a slight increase before reaching stability. Sugarcane bagasse contains a moderate amount of lignin, which slows the breakdown of silica-rich components [18, 19]. Beyond 90 minutes, silica continues to be gradually released, leading to fluctuations rather than complete stabilization.

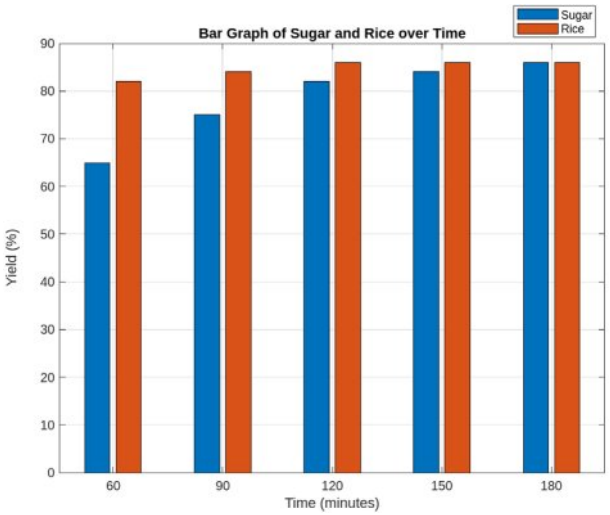

Fig. 3. Effect of time.

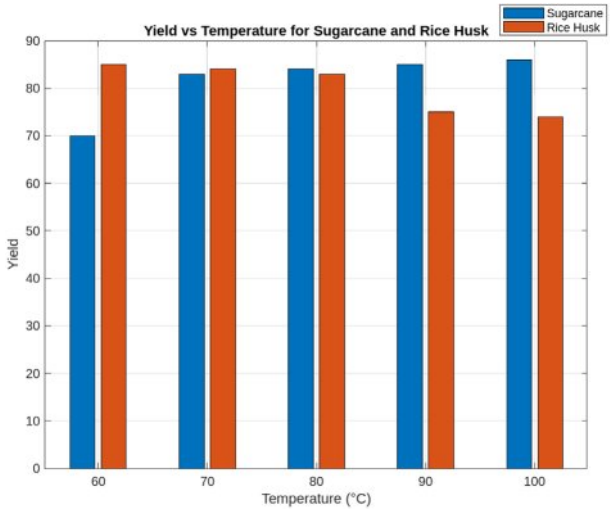

Fig. 5. Effect of Temperature.

Additionally, variations in cellulose, hemicellulose, and lignin proportions across different biomass sources may result in inconsistent silica release rates, causing fluctuations as different fractions are extracted at varying times [18, 19]. These variations in silica yield after 90 minutes suggest that extraction is still ongoing, likely due to the gradual breakdown of the sugarcane bagasse structure and the continued release of silica-rich compounds rather than reaction saturation or degradation effects.

Effect of Amount of Solvent

Fig. 4 depicts the relationship between NaOH concentration and silica extraction yield. The yield reaches its maximum at 400 ml of NaOH with 10 g of both IRA and sugarcane bagasse ash. Beyond which minor fluctuations (~±2%) are observed. These fluctuations can be explained by the solubility equilibrium of silica in an alkaline medium. When the NaOH concentration surpasses the optimal threshold, additional base may lead to excessive polymerization of silica, forming denser silica gels that do not contribute effectively to nanoparticle yield [20]. To ensure clarity, the yield percentage is reported as % w/w (weight of silica extracted per initial biomass weight). This unit provides a standardized measure of efficiency, making comparisons between different conditions more precise.

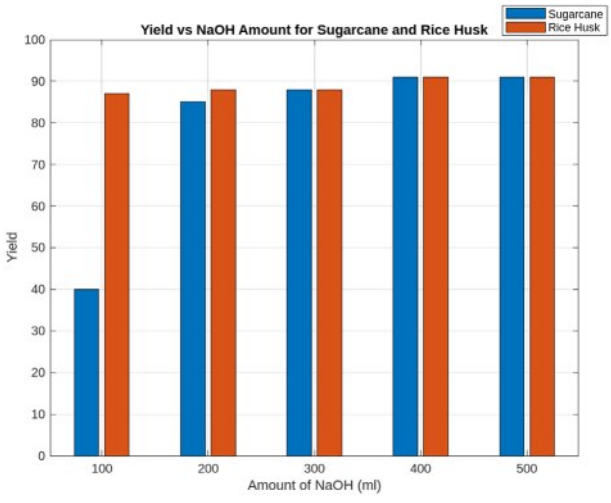

Fig. 4. Effect of Amount of Solvent.

Effect of Temperature

Figure 5 illustrates the effect of temperature on silica yield. Experiments were conducted in 10 °C increments, covering a temperature range from 50 °C to 100 °C. The results indicate that the optimal silica yield was obtained at 60 °C for immature rice and 100 °C for sugarcane bagasse. This trend suggests that lower temperatures are sufficient for immature rice due to its higher silica solubility, whereas sugarcane bagasse requires higher temperatures to break down its more complex organic matrix and facilitate silica release [21, 22]. Beyond 100 °C, further increases in temperature resulted in minimal improvements in yield, indicating a plateau effect where additional heating no longer enhances extraction efficiency.

Characterization

The following figures illustrate the various characterizations of sugarcane bagasse ash, including FTIR, XRD and SEM.

FTIR of silica nanoparticles obtained from SBA:

The Fig. 6 explains the FTIR spectrum provides molecular insights into the extracted silica nanoparticles. Key vibrational modes confirm the presence of well-formed silica: 3421 cm^{-1} – Broad O-H stretching from silanol (-Si-OH) groups, indicative of surface hydroxylation, which enhances reactivity. 1636 cm^{-1} – Bending vibrations of adsorbed H_2O, suggesting residual moisture within the silica structure. 1050 cm^{-1}

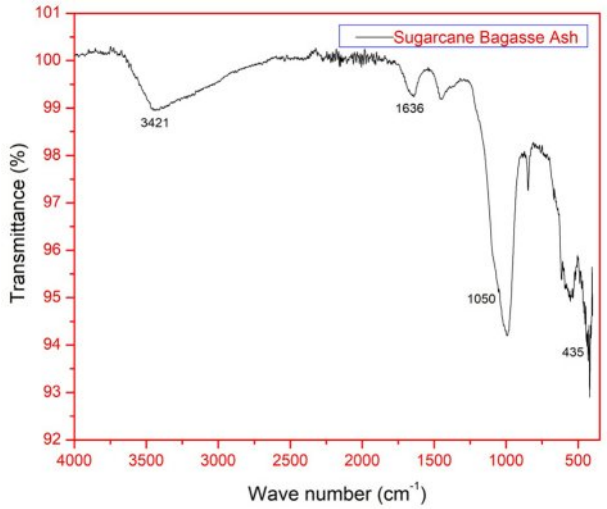

Fig. 6. FTIR of silica nanoparticles obtained from sugarcane bagasse ash.

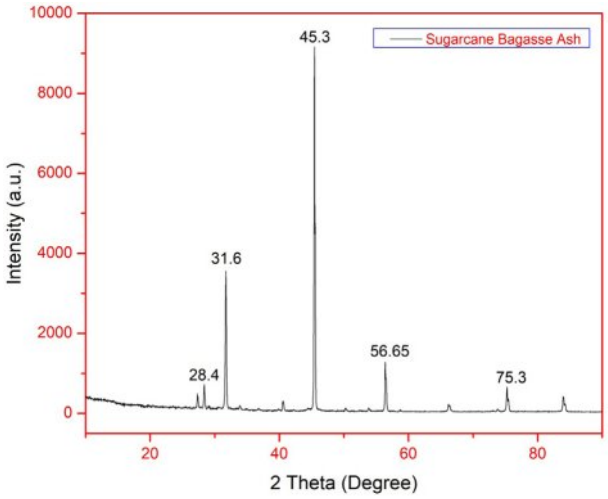

Fig. 7. XRD of silica nanoparticles obtained from sugarcane bagasse ash.

– Asymmetric stretching of Si-O-Si bonds, characteristic of a silica network. 793 cm^{-1} – Symmetric Si-O-Si stretching, confirming tetrahedral silica units. 436 cm^{-1} – Si-O-Si bending vibrations, further validating silica formation. The presence of well-defined peaks at these positions confirms the formation of high-purity silica nanoparticles [23].

XRD of silica nanoparticles obtained from SBA:

The XRD spectrum exhibits distinct diffraction peaks at 2θ = 20.9° to 26.6°, indicating the presence of crystalline silica (quartz phase). However, the broad peaks suggest that some amorphous silica is also present alongside the crystalline phases, indicating partial crystallinity rather than a fully amorphous structure. The Full Width at Half Maximum (FWHM) values were calculated using Bragg's Law (FWHM (β) = 0.0118 nm, λ = 0.154 nm, θ = 0.232 radians). The Scherrer equation was then applied to determine the crystalline domain size [24].

The Scherrer equation

$$D = (0.94 \times \lambda) / (\beta \times \cos\theta) = 12.45\text{nm}$$

Where:

D = Average crystallite size,
λ = X-ray wavelength,

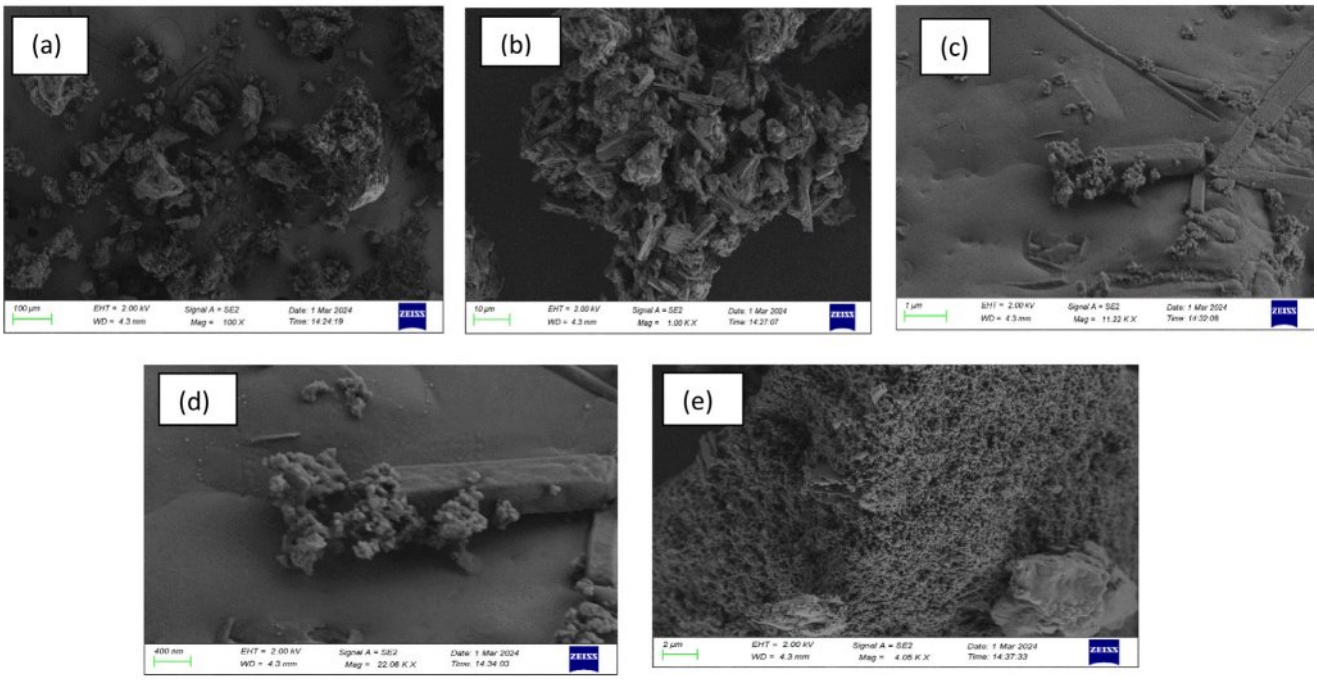

Fig. 8. (a), (b), (c), (d), (e) SEM Analysis of silica nanoparticles obtained from sugarcane bagasse ash.

β = Full Width at Half Maximum (FWHM) in radians,
θ = Bragg angle.

SEM Analysis of silica nanoparticles obtained from SBA

The SEM images reveal spherical silica nanoparticles with smooth surfaces. The nanoparticles appear uniformly distributed with minimal agglomeration, and their sizes fall within the nanoscale range. The well-dispersed nature of the particles indicates a successful sol-gel synthesis method. Some degree of clustering is visible, which is expected due to the high surface energy of nanoparticles. However, the particles remain relatively discrete, confirming good synthesis control. The particle size was determined using image processing software (Image J), with a measured size range of 12–23 nm. The degree of agglomeration (DA) can be estimated using the following formula: $DA=D_{SEM} / D_{XRD}$

Where: D_{SEM} = Average particle size from SEM analysis (measures agglomerated clusters) D_{XRD} = Crystallite size from Scherrer equation (XRD) (measures primary particle size)

D_{SEM} = 12-23 nm = 17.5 nm, D_{XRD} = 12.45 nm

DA=17.4/12.45 =1.4

SBA Silica (DA=1.4) Slight Agglomeration (Good dispersion)

Characterization

The following figures illustrate the various characterizations of immature rice ash, including FTIR, XRD and SEM.

FTIR of silica nanoparticles obtained from IRA

From the Fig. 9 the peak at 796.4 cm^{-1} (O–Si–O symmetric vibration) indicates the presence of Si–O–Si bonds, a hallmark of the silica network. It is directly tied to the well-formed, ordered structure of the silica nanoparticles. 1052 cm^{-1} (O–Si–O asymmetric vibration): This peak represents the O–Si–O asymmetric stretching vibration. The presence of this peak further supports the formation of a silica network. In well-formed silica nanoparticles, these asymmetric vibrations are indicative of the bridging oxygen atoms between silicon atoms 966.2 cm^{-1} (Si–OH bending and stretching vibrations): The appearance of a sharp peak at 966.2 cm^{-1} is significant, as it is related to the bending and stretching vibrations of Si–OH bonds. The presence of this peak points to the surface hydroxyl groups present on the silica nanoparticles. The sharpness of the peak further suggests that these surface hydroxyl groups are well-defined, reinforcing the idea of a high-quality silica nanoparticle with a clean and well-controlled surface structure. 1634 cm^{-1} (H–O–H bending vibration): The peak at 1634 cm^{-1} confirms the presence of adsorbed water molecules on the surface of the silica nanoparticles. In summary,

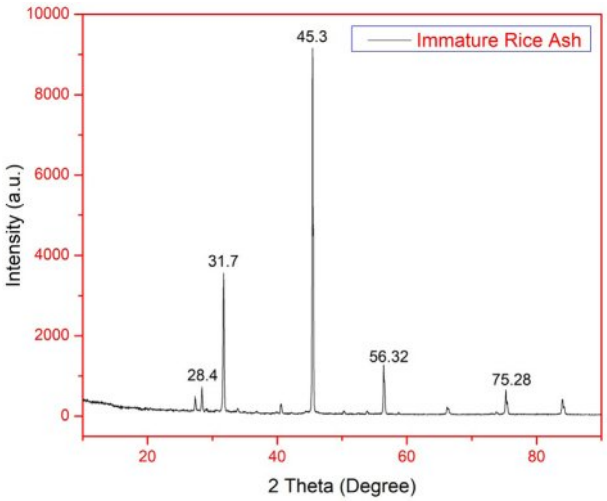

Fig. 9. FTIR of silica nanoparticles obtained from immature rice ash.

the FT-IR spectrum clearly indicates the formation of well-structured silica nanoparticles, as evidenced by the characteristic O–Si–O vibrations at 796.4 cm^{-1} and 1052 cm^{-1}, the presence of Si–OH surface groups at 966.2 cm^{-1}, and the signature of adsorbed water at 1634 cm^{-1}. These peaks are all consistent with a well-formed silica nanoparticle network with a well-defined surface and hydration state [25].

XRD of silica nanoparticles obtained from IRA

The XRD pattern exhibits a broad "halo" between 2θ = 15° and 30°, which is a strong indicator of amorphous silica. The absence of sharp diffraction peaks suggests that the silica structure lacks long-range order, confirming its amorphous nature. This characteristic is expected for biogenic silica, as it forms through natural plant processes, resulting in irregular atomic arrangements

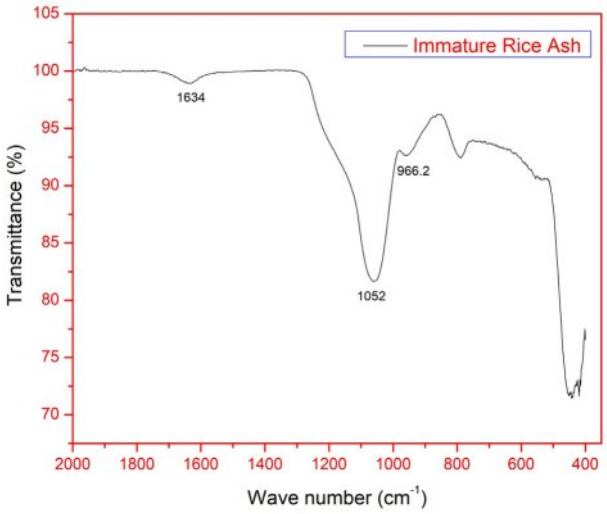

Fig. 10. XRD of silica nanoparticles obtained from immature rice ash.

rather than a well-defined crystalline structure. The Full Width at Half Maximum (FWHM) values were calculated using Bragg's Law (FWHM (β) = 0.00819 nm, λ = 0.154 nm, θ = 0.192 radians). The Scherrer equation was then applied to determine the crystalline domain size, yielding a value of D = 18.0 nm.

SEM Analysis of silica nanoparticles obtained from IRA

The silica nanoparticles derived from IRA also exhibit a spherical structure, similar to those obtained from sugarcane bagasse ash. The images show a slightly wider size range, indicating that some polydispersity exists. The particles are found within the 49–91 nm range, slightly larger than those from sugarcane bagasse ash [26, 27]. This SEM analysis was done before grinding the extracted silica that may be reason of large size range or due to differences in silica extraction efficiency from rice ash. This also could be due to the higher surface hydroxyl groups (Si-OH), leading to hydrogen bonding between particles. The particle size range was determined by using Image processing software. Particle size range = 49-91 nm.

The degree of agglomeration (DA) can be estimated using the following formula:

$$DA = D_{SEM} / D_{XRD}$$

Where:

- D_{SEM} = Average particle size from SEM analysis (measures agglomerated clusters)
- D_{XRD} = Crystallite size from Scherrer equation (XRD) (measures primary particle size)

D_{SEM} = 49-91 nm = 70 nm
D_{XRD} = 18 nm
DA=3.9

IRA Silica (DA=3.9) High Agglomeration (Significant clustering)

Conclusions

This research successfully demonstrated an eco-friendly method for synthesizing silica nanoparticles from SBA and IRA using the sol-gel technique. The approach not only provides a sustainable waste management solution but also yields high-purity Nano silica, making it suitable for various applications. The characterization studies confirmed the structural and morphological properties of the synthesized nanoparticles SEM analysis revealed spherical and well-dispersed nanoparticles with minimal agglomeration. XRD analysis indicated that sugarcane bagasse-derived silica contained both crystalline and amorphous phases, while immature rice-derived silica was primarily amorphous, with particle sizes ranging from 12–23 nm (XRD) and 49–91 nm (SEM). FTIR results verified the formation of silica networks, with characteristic Si-O-Si bond vibrations confirming the purity of the material. The findings of this study highlight a cost-effective and environmentally sustainable method for producing Nano silica from agricultural residues. These nanoparticles have potential applications in nanocomposites, catalysis, pollution control, Nano-fertilizers, and biomedical fields

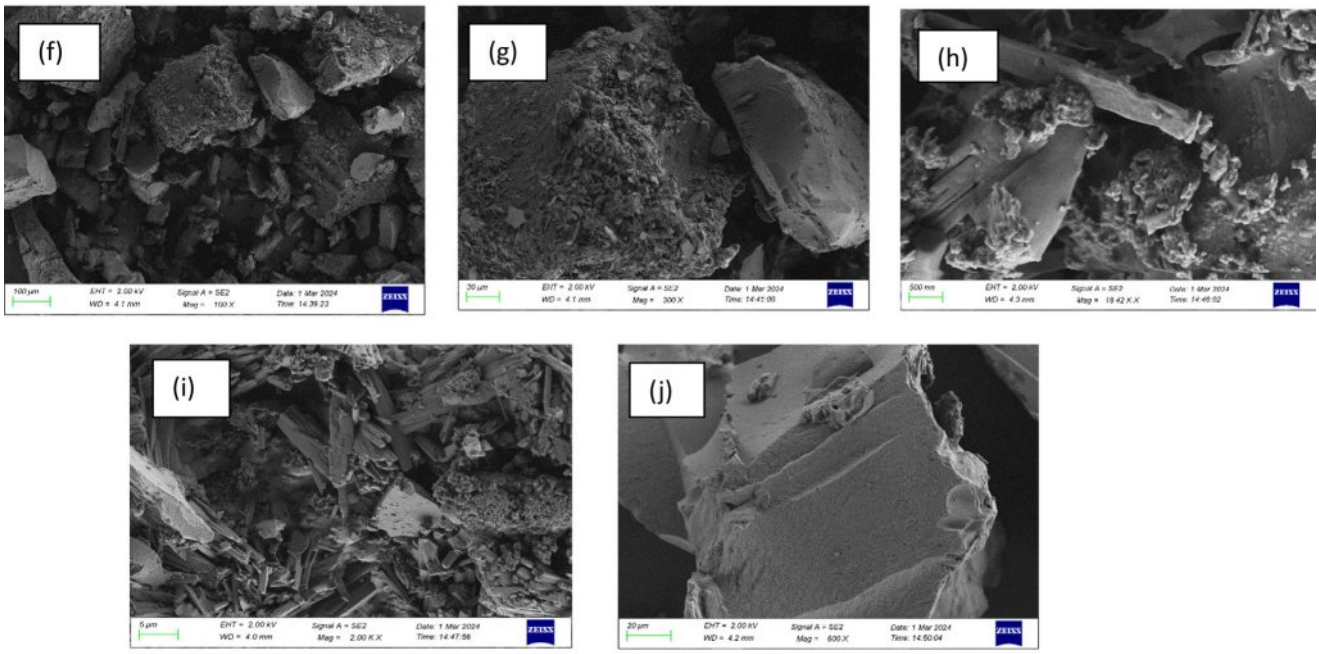

Fig. 11. (f), (g), (h), (i), (j) SEM Analysis of silica nanoparticles obtained from immature rice ash.

References

1. B. Koul, M. Yakoob, and M.P. Shah, Environ. Res. 206 (2022) 112285.
2. A. Pandey, C.R. Soccol, P. Nigam, and V.T. Soccol, Bioresour. Technol. 74 (2000) 69-80.
3. Y. Li, J. Chai, R. Wang, X. Zhang, and Z. Si, J. Build. Eng. 56 (2022) 104774.
4. Y. Sun and J. Cheng, Bioresour. Technol. 83 (2002) 1-11.
5. B. Gadde, S. Bonnet, C. Menke, and S. Garivait, Environ. Pollut. 157 (2009) 1554-1558.
6. S. Kumar Das, A. Adediran, C. Rodrigue Kaze, S. Mohammed Mustakim, and N. Leklou, Constr. Build. Mater. 345 (2022) 128341.
7. A.A. Raheem and M.A. Kareem, Int. J. Eng. Res. Afr. 32 (2017) 25-35.
8. ResearchGate (2025).
9. T.G. Korotkova, S.J. Ksandopulo, A.P. Donenko, S.A. Bushumov, and A.S. Danilchenko, Orient. J. Chem. 32 (2016) 3213-3219.
10. U. Kalapathy, A. Proctor, and J. Shultz, Bioresour. Technol. 73 (2000) 257-262.
11. I. Kouadri, B.B. Seghir, H. Hemmami, S. Zeghoud, N. Allag, A. Rebiai, I.B. Amor, A. Chala, and H. Belkhalfa, Asian J. Res. Chem. (2023) 97.
12. S.S. Nekrashevich and V.A. Gritsenko, Phys. Solid State 56 (2014) 207-222.
13. F. Weinhold and R. West, Organometallics 30 (2011) 5815-5824.
14. C.J. Brinker and G.W. Scherer, Sol-Gel Science: The Physics and Chemistry of Sol-Gel Processing, Academic Press, 2013.
15. U. Simon, Angew. Chem. Int. Ed. 43 (2004) 5723-5723.
16. I.A. Rahman, and V. Padavettan, J. Nanomater. 2012 (2012) 132424.
17. I.U. Haq and K.A.A. Malik, J. Chem. Soc. Pak. 36 (2014) 382.
18. S. Palakurthy, L. Houben, M. Elbaum, and R. Elbaum, Biomacromolecules 25 (2024) 3409-3419.
19. I. Hamidu, B. Afotey, B. Kwakye-Awuah, and D.A. Anang, Heliyon 11 (2025) e42491.
20. S. Bhakta, C.K. Dixit, I. Bist, K.A. Jalil, S.L. Suib, and J.F. Rusling, Mater. Res. Express 3 (2016) 075025.
21. I.J. Fernandes, D. Calheiro, F.A.L. Sánchez, A.L.D. Camacho, T.L.A.D.C. Rocha, C.A.M. Moraes, and V.C.D. Sousa, Mater. Res. 20 (2017) 519-525.
22. N.S. Seroka, R. Taziwa, and L. Khotseng, Nanomaterials 12 (2022) 2184.
23. G. Falk, G.P. Shinhe, L.B. Teixeira, E.G. Moraes, and A.P.N. de Oliveira, Ceram. Int. 45 (2019) 21618-21624.
24. Y.L. Nimah, Z.H. Muhaiminah, and S. Suprapto, Nanoparticle 4 (2023) 1-5.
25. D. Dorairaj, N. Govender, S. Zakaria, and R. Wickneswari, Sci. Rep. 12 (2022) 20162.
26. H.S. Lee, S.M. Koo, and J.W. Yoo, J. Ceram. Process. Res. 13[2] (2012) s300-s303.
27. P. Sudha, S. Ramesh, R. Jagadeesan, and K. Yuvaraj, J. Ceram. Process. Res. 25[1] (2024) 1-15.